Universal metabolic constraints on the thermal tolerance of marine phytoplankton

Samuel Barton[1*], James Jenkins[1], Angus Buckling[1], C.-Elisa Schaum[1], Nicholas Smirnoff[2] & Gabriel Yvon-Durocher[1*]

[1] Environment and Sustainability Institute, University of Exeter, Penryn Campus, Penryn, Cornwall TR10 9EZ, UK,

[2] Biosciences, College of Life and Environmental Sciences, Geoffrey Pope Building University of Exeter, Exeter, EX4 4QD, UK

*for correspondence, email: G.Yvon-Durocher@exeter.ac.uk , sb384@exeter.ac.uk

Words in summary: 259

Words in main text: 2231

Number of Figures (main text): 4

Number of Tables (main text): 0

Marine phytoplankton are responsible for over 45% of annual global net primary production[1–4]. Ocean warming is expected to drive massive reorganisation of phytoplankton communities, resulting in pole-ward range shifts and sharp declines in species diversity, particularly in the tropics[5–8]. The impacts of warming on phytoplankton species depend critically on their physiological sensitivity to temperature change, characterised by thermal tolerance curves[5,9]. Local extinctions arise when temperatures exceed species' thermal tolerance limits[5]. The mechanisms that determine the characteristics of thermal tolerance curves (e.g. optimal and maximal temperatures) and their variability among the broad physiological diversity of marine phytoplankton are however poorly understood[10,11]. Here we show that differences in the temperature responses of photosynthesis and respiration establish physiological trade-offs that constrain the thermal tolerance of 18 species of marine phytoplankton, spanning cyanobacteria as well as the red and green super-families[12,13]. Across all species we found that rates of respiration were more sensitive to increasing temperature and typically had higher optimal temperatures than both photosynthesis and growth. Consequently, the respiratory cost of growth increased exponentially with rising temperatures eventually exceeding the supply of reduced carbon from photosynthesis, causing performance to decline rapidly past an optimum temperature. Our findings suggest that declines in performance at temperatures exceeding the optimum reflect diversion of metabolic energy away from growth to accommodate exponentially increasing costs of repair and maintenance likely driven by heat-induced cellular damage. These highly conserved patterns demonstrate that the limits of thermal tolerance in marine phytoplankton are underpinned by common metabolic constraints linked to the differential temperature responses of photosynthesis and respiration.

The planet's oceans are changing at an unprecedented rate[14]; over the past half-century average sea surface temperatures have been increasing by 0.1 ºC per decade[15] and are projected to rise by a further 3ºC or more by the end of the century[16]. Ocean warming is thought to be a key driver of recent declines in phytoplankton productivity[17–19], and models of marine biogeochemistry predict further reductions in productivity over the 21st century as temperatures exceed limits of thermal tolerance and nutrient limitation increases in warmer, more stratified oceans[20]. Thermal tolerance curves of marine phytoplankton (like all ectotherms) exhibit characteristic unimodality and left-skew, meaning that fitness declines more sharply above the optimum temperature than below[5]. Marine phytoplankton species

exhibit substantial variability in their thermal tolerance. Optimal temperatures for growth range between approximately 2 to 38ºC and are positively correlated with the average temperature of the environment, indicating a global pattern of thermal adaptation[5,21]. Ocean warming is expected to result in major reorganisation of marine phytoplankton communities as temperatures exceed the thermal optima of some species but not others. In particular, tropical and sub-tropical regions are projected to experience pronounced declines in species diversity and productivity[5,21] because many of the taxa in these areas already exist close to their limits of thermal tolerance. Despite its importance for predicting the impacts of global warming on marine phytoplankton, we currently understand very little about the physiological processes that determine the limits of thermal tolerance in marine phytoplankton.

To address this fundamental knowledge gap we carried out a large-scale experiment to investigate the physiological mechanisms that set the limits of thermal tolerance in marine phytoplankton. Our experiments span a representative sample of the broad physiological and phylogenetic diversity of the marine phytoplankton; including 18 species belonging to ecologically important functional groups – Cyanobacteria, Diatoms, Dinoflagellates, Coccolithophores, Rhodophytes, Chlorophytes and Prasinophytes (Table S1). These species were chosen to encompass the putative primary and secondary endosymbionts of both the red and green super-families, and thus reflect the complex evolutionary histories of marine phytoplankton[12,13]. This allowed for us to investigate whether, in spite of such physiological diversity in plastid evolution, similar physiological constraints underpin the limits of thermal tolerance.

We first characterised variability in thermal tolerance curves among taxa by measuring growth rates for each species across a temperature gradient spanning 15 to 37°C and fitting the Sharpe-Schoolfield equation for high temperature inactivation to the data using non-linear mixed effects modelling[22,23] (Fig.1). The upper limits of thermal tolerance varied across the taxa, with ${T_{max}}^{\mu}$ (maximum temperature of observed growth), ranging from 27°C to 37°C. The optimal temperature of growth, ${T_{opt}}^{\mu}$, ranged from 23.8°C to 34.0°C and the activation energy, ${E_a}^{\mu}$ – which characterises the increase in rate up to ${T_{opt}}^{\mu}$ – ranged from 0.40 eV to 1.46 eV, with an average ${E_a}^{\mu}$ of 0.77eV (95% CI: 0.58 to 0.97) (Fig.1, and Table 2, SI). These ${E_a}^{\mu}$ values highlight that the temperature dependence of growth at the species level is significantly higher than previously reported temperature dependence parameters,

such as the canonical Eppley coefficient (equivalent to ${E_a}^{\mu} \approx$ 0.3 eV), that are derived by comparing maximum growth rates across many species and are the standard way in which the impacts of warming on phytoplankton productivity are represented in models of marine biogeochemistry[24–26]. These findings suggest that the Eppley coefficient (and other values from similar analyses[26]), which capture the broad-scale, macroecological impacts of temperature along geographic gradients, might significantly under estimate the impacts of temperature fluctuations on phytoplankton growth at local to regional scales (see Supplementary Information S5 for further discussion).

To determine the physiological processes that shape the thermal tolerance curves, in particular those that determine the optimum temperature and supra-optimal declines in growth rate, it is essential to understand how the key metabolic pathways that drive biomass synthesis respond to warming. Despite having diverse evolutionary histories, all unicellular phytoplankton share common, key metabolic pathways[27] and their ability to sequester carbon, and therefore grow, is ultimately determined by photosynthesis and respiration[28,29]. The light-dependent reactions of photosynthesis account both for the processes that convert inorganic carbon to organic carbon stores and those that facilitate the production of ATP and reductant used to fuel biomass synthesis[30]. The dark reactions in respiration can be conceptually divided into 'growth' and 'maintenance' components[28–31]. 'Growth-respiration' provides the ATP, reductant and carbon skeletons required for producing new biomass and is expected to be proportional to the rate of growth. By contrast, 'maintenance-respiration' provides the ATP for macromolecular turnover and the maintenance of solute gradients, and is proportional to cell biomass[30]. To understand the physiological trade-offs that shape the variability in phytoplankton thermal tolerance, we simultaneously quantified temperature-dependent variation in rates of photosynthesis and respiration alongside the thermal response curve of growth rate in the 18 species of marine phytoplankton.

Below the optimal temperature for growth, ${T_{opt}}^{\mu}$, we found that net photosynthesis was directly proportional to growth rate across all species ($\chi^2 = 14.1,\ p < 0.005$), with an average slope of $\emptyset^{NP}$ = 1.23 (the net photosynthesis cost of biosynthesis, 95% CI: 0.54 to 1.95 , Fig.2). Dark respiration was also proportional to growth ($\chi^2 = 15.93,\ p < 0.005$) with an average slope across all species of $\emptyset^{R}$ = 0.75 (95% CI: 0.44 to 1.06, Fig.2) and was tightly coupled to rates of photosynthesis ($\chi^2 = 28.2,\ p < 0.005$), with approximately 33% of the carbon fixed by gross photosynthesis accounted for by dark respiration (Fig. S4A).

These findings indicate that at temperatures at or below ${T_{opt}}^{\mu}$ the majority of the energy used to fuel biomass synthesis comes primarily from photosynthesis. Nonetheless, the coupling between growth and dark respiration suggests that some of the reductant for biosynthesis is also derived from respiration. Indeed, the average value for the estimated respiratory cost of biosynthesis, $\emptyset^R$ (the slope of the relationship between dark respiration and growth), was statistically indistinguishable from the theoretical value of 0.67 for the costs of biosynthesis when nitrate is the nitrogen source[28] and is in line with previous work showing that $\emptyset^R$ can range from approximately 0.1 to 1.0 in unicellular algae[31]. At temperatures below ${T_{opt}}^{\mu}$, rates of growth, photosynthesis and dark respiration are clearly tightly coupled indicating that the majority of the measured dark respiration is 'growth-respiration' and fuels ATP production for biomass synthesis. However when temperatures exceed ${T_{opt}}^{\mu}$, we found that the tight coupling between growth, photosynthesis and dark respiration broke down; neither rates of net photosynthesis (Fig. 2C; $\chi^2 = 0.31,\ p = 0.58$) or respiration (Fig. 2F; $\chi^2 = 0.20,\ p = 0.65$) were significantly correlated with growth past ${T_{opt}}^{\mu}$. These findings suggest that differences in the thermal sensitivities of photosynthesis, respiration and growth might play a key a role in constraining the thermal tolerance curve and determining supra-optimal declines in growth rates.

For each species, we measured the responses of gross photosynthesis and dark respiration across a temperature gradient spanning 7°C to 50°C, and quantified the resultant thermal response curves by fitting the Sharpe-Schoolfield equation for high temperature inactivation to the data using non-linear mixed effects modelling (see Methods). We found consistent differences in the parameters characterising the thermal responses of photosynthesis and respiration across all the species in this study despite their diverse evolutionary histories (Fig.3, Fig. S2 and S3). The activation energy for respiration was greater than that of photosynthesis (i.e. ${E_a}^R > {E_a}^P$; Fig. 3B, Fig. S2 and S3) in all 18 species. Pooling the parameters across species yielded an average activation energy for photosynthesis of ${E_a}^P$= 0.70 eV (95% CI: 0.63 to 0.77), whilst the average for respiration was ${E_a}^R$ = 1.01 eV (95% CI: 0.93 to 1.09). Critically, the average activation energy for photosynthesis was statistically indistinguishable from that of growth rate (${E_a}^{\mu}$ = 0.77eV, 95% CI: 0.58 to 0.97). Owing to the stronger temperature-dependence of respiration, these results demonstrate that respiratory costs become an increasingly large proportion of photosynthetic carbon fixation and biomass synthesis as temperatures rise toward the peak of the thermal

response curves. We also found that for most species, the optimum temperature for respiration was higher than that of photosynthesis (i.e. $T_{opt}{}^{R} > T_{opt}{}^{P}$), with the average thermal optimum for photosynthesis, $T_{opt}{}^{P}$ = 31.7°C ± 0.86 (s.e.m.) and respiration, $T_{opt}{}^{R}$ = 33.2°C ± 0.62 (s.e.m.) (Fig. 3C, Fig. S2 and S3). Furthermore, in all species, the deactivation energy, which characterises the speed that rates decline past the optimum, was lower for respiration relative to photosynthesis (i.e. $E_h{}^{P} > E_h{}^{R}$), with the average across species for photosynthesis $E_h{}^{P}$ = 6.92 (95% CI: 5.75 to 8.09) and respiration $E_h{}^{R}$ = 3.04 (95% CI: 2.46 to 3.61) (Fig. 3D, Fig. S2 and S3). These results indicate that as temperatures rise beyond T_{opt}, rates of photosynthesis decline faster than rates of respiration. This result, combined with the lower T_{opt} of photosynthesis, suggests a weaker thermal tolerance of the photosynthetic machinery[32]. Overall these findings show remarkable consistency across diverse taxa (Fig. S2 and S3) in how differences in the parameters that characterise the thermal responses of photosynthesis and respiration result in increasing respiratory expenditure of carbon fixed by photosynthesis as temperatures rise..

To determine whether the differential thermal responses of growth, photosynthesis and respiration can help explain the physiological processes that constrain the thermal tolerance curves of diverse phytoplankton, we used a simple model[31], along with the measurements of growth and respiration, to estimate how the respiratory cost of biosynthesis, $\emptyset^{R}$, varied as a function of temperature

$$\emptyset^{R}(T) = R(T) - R_0 / \mu(T) \qquad (1)$$

where $R(T)$ is the rate of R at growth temperature, T, μ is the mean growth rate at T , and R_0 is the maintenance-respiration rate when $\mu = 0$. Thus, whenever $E_a{}^{R} > E_a{}^{\mu}$ and/or $T_{opt}{}^{R} > T_{opt}{}^{\mu}$ the respiratory cost of biosynthesis, $\emptyset^{R}$, is expected to increase with rising temperatures. To explicitly test this hypothesis we quantified the temperature-dependence of $\emptyset^{R}$ using the Arrhenius equation fitted via a linear mixed effects model, which enables us to characterise the average temperature response across all taxa as well as the species-specific deviations from the average temperature response. Across all 18 species, $\emptyset^{R}$ increased exponentially with rising temperatures ($\chi^2 = 30.0,\ p < 0.005$). The activation energy characterising the temperature dependence of $\emptyset^{R}$ was remarkably consistent across the 18 species, with $E_a{}^{\emptyset^{R}}$ ranging between 0.37 to 0.72 eV and an average across species of 0.57eV (95% CI: 0.44 to 0.70, Fig.4). This result suggests that declines in growth rate past the

optimum are driven by exponentially increasing respiratory costs that eventually exceed the supply rate of reduced substrates from photosynthesis. Furthermore, it is likely that these increased respiratory costs could be associated with repairing heat-induced damage to the photosynthetic machinery, which have a much lower thermal tolerance than the respiratory apparatus (see Fig. 3; lower T_{opt}, higher E_h).

Overall, our findings highlight marked similarities in the physiological trade-offs that underpin the thermal tolerance of marine phytoplankton across diverse taxonomic groups, spanning the cyanobacteria and red and green super families. We found that rates of respiration were more sensitive to temperature, had higher thermal optima and declined less abruptly past the optimum than those of photosynthesis. At sub-optimal temperatures photosynthesis, respiration and growth were tightly coupled indicating that both dark respiration and photosynthesis provide ATP and reductant for biosynthesis. At high temperatures however, photosynthesis, respiration and growth became markedly decoupled, with respiratory costs rising exponentially with increasing temperature relative to growth and photosynthesis. These patterns suggest that universal metabolic constraints driven by the differential temperature sensitivity of photosynthesis, respiration and growth shape the limits of thermal tolerance of diverse marine phytoplankton.

Our experiments were conducted under light and nutrient replete conditions. Recent work has shown that both the temperature sensitivities of photosynthesis and respiration[33], and the optimal temperature for growth[34] tend to decline under nutrient and light limitation[35,36]. Whilst the absolute values of the thermal sensitivities of photosynthesis and respiration may indeed decline under resource limitation, we expect that the supra-optimal declines in growth linked to temperature-driven decoupling between photosynthesis, respiration and biomass synthesis that we have shown here, will apply equally under resource replete and limited conditions. Indeed, previous work has shown that while light limitation constrains the temperature response of net photosynthesis, respiration remains strongly temperature-dependent[35]. Thus, temperature-driven decoupling between respiration, photosynthesis growth is likely to be amplified under resource (nutrient and/or light) limitation, providing further support for recent observations of lower thermal tolerance in marine phytoplankton under nutrient limited conditions[34].

Recent work has also provided anecdotal evidence that a handful of species of marine and freshwater phytoplankton can rapidly evolve tolerance to temperatures in excess of their

contemporary thermal optima[10,11,37,38] and that thermal adaptation is associated with changes in photosynthetic and respiratory traits that increase carbon allocation to growth under high temperature[11,38]. Our findings indicate that evolutionary adjustments in metabolic traits that increase carbon allocation to growth, and compensate for the differential temperature sensitivities of photosynthesis and respiration, could be common feature of rapid adaptation to warming across the broad physiological diversity of marine phytoplankton owing to universal metabolic constraints on thermal tolerance. These results therefore help pave the way for improving representations of phytoplankton biodiversity in models of ocean biogeochemistry by providing a process-based understanding of the factors that shape the limits of temperature tolerance for diverse species of marine phytoplankton, which can be used to aid predictions of immigration and local extinctions driven by global warming.

References

1. Field, C. B., Behrenfeld, M. J., Randerson, J. T. & Falkowski, P. Primary Production of the Biosphere: Integrating Terrestrial and Oceanic Components. *Science,* **281,** 237–240 (1998).

2. Falkowski, P. G., Fenchel, T. & Delong, E. F. The Microbial Engines That Drive Earth's Biogeochemical Cycles. *Science,* **320,** 1034–1039 (2008).

3. Sunagawa, S. *et al.* Structure and function of the global ocean microbiome. *Science,* **348,** 1261359–1/9 (2015).

4. de Vargas, C. *et al.* Eukaryotic plankton diversity in the sunlit ocean. *Science,* **348,** 1261605–1/11 (2015).

5. Thomas, M. K., Kremer, C. T., Klausmeier, C. a. & Litchman, E. A Global Pattern of Thermal Adaptation in Marine Phytoplankton. *Science,* **338,** 1085–1088 (2012).

6. Follows, M. J., Dutkiewicz, S., Grant, S. & Chisholm, S. W. Emergent Biogeography of Microbial Communities in a Model Ocean. *Science,* **315,** 1843–1846 (2007).

7. Barton, A. D., Dutkiewicz, S., Flierl, G., Bragg, J. & Follows, M. J. Patterns of Diversity in Marine Phytoplankton. *Science,* **327,** 1509–1511 (2010).

8. Norberg, J., Urban, M. C., Vellend, M. *et al,* Eco-evolutionary responses of biodiversity to climate change. *Nat. Clim. Chang,* **2,** 747–751 (2012).

9. Boyd, P. W. *et al.* Marine Phytoplankton Temperature versus Growth Responses from Polar to Tropical Waters - Outcome of a Scientific Community-Wide Study. *PLoS One* **8** (2013).

10. Schaum, C.-E. *et al.* Adaptation of phytoplankton to a decade of experimental warming linked to increased photosynthesis. *Nat. Ecol. Evol.* **1,** 0094 (2017).

11. Padfield, D., Yvon-Durocher, G., Buckling, A., Jennings, S. & Yvon-Durocher, G. Rapid evolution of metabolic traits explains thermal adaptation in phytoplankton. *Ecol. Lett.* **19,** 133–142 (2016).

12. Falkowski, P. G. *et al.* The Evolution of Modern Eukaryotic. *Science,* **305,** 354–360 (2004).

13. Keeling, P. J. Diversity and evolutionary history of plastids and their hosts. *Am. J. Bot.* **91,** 1481–1493 (2004).

14. Henson, S. A. *et al.* Rapid emergence of climate change in environmental drivers of marine ecosystems. *Nat. Commun.* **8,** 1–9 (2017).

15. Rhein, M. *et al.* Observations: Ocean Pages. In *Climate Change 2013: The Phyical. Science Basis. Contribution to Working Group I to the Fifth Assessment Report of the Intergovernmental Panel on Climate Change.* Cambridge University Press, Cambridge, UK and New York, 255–316 (2013).

16. Collins, M. *et al.* Long-term Climate Change: Projections, Commitments and Irreversibility. In *Climate Change 2013: The Phyical. Science Basis. Contribution to Working Group I to the Fifth Assessment Report of the Intergovernmental Panel on Climate Change.* Cambridge University Press, Cambridge, UK and New York, 1029–1136 (2013).

17. Boyce, D. G., Lewis, M. R. & Worm, B. Global phytoplankton decline over the past century. *Nature,* **466,** 591–596 (2010).

18. Behrenfeld, M. J. *et al.* Climate-driven trends in contemporary ocean productivity. *Nature,* **444,** 752–755 (2006).

19. Capuzzo, E. *et al.* A decline in primary production in the North Sea over 25 years, associated with reductions in zooplankton abundance and fish stock recruitment. *Glob. Chang. Biol.* **24,** e352–e364 (2018).

20. Laufkotter, C. *et al.* Drivers and uncertainties of future global marine primary production in marine ecosystem models. *Biogeosciences,* **12,** 6955–6984 (2015).

21. Thomas, M. K., Kremer, C. T. & Litchman, E. Environment and evolutionary history determine the global biogeography of phytoplankton temperature traits. *Glob. Ecol. Biogeogr.* **25,** 75–86 (2016).

22. Sharpe, P. J. H. & DeMichele, D.W. Reaction Kinetics of Poikilotherm Development. *J. Theor. Biol.* **64,** 649–670 (1977).

23. Schoolfield, R. M., Sharpe, P. J. H. & Magnuson, C. E. Non-linear regression of biological temperature-dependent rate models based on absolute reaction-rate theory. *J. Theor. Biol.* **88,** 719–731 (1981).

24. Eppley, R. W. Temperature and phytoplankton growth in the sea. *Fish. Bull.* **70,** 1063–1085 (1972).

25. Chen, B. & Laws, E. A. Is there a difference of temperature sensitivity between marine phytoplankton and heterotrophs? *Limnol. Oceanogr.* **62,** 806–817 (2017).

26. Kremer, C. T., Thomas, M. K. & Litchman, E. Temperature- and size-scaling of phytoplankton population growth rates: Reconciling the Eppley curve and the metabolic theory of ecology. *Limnol. Oceanogr.* **62,** 1658–1670 (2017).

27. Quigg, A. *et al.* The evolutionary inheritance of elemental stoichiometry in marine phytoplankton. *Nature* **425,** 291–4 (2003).

28. Shuter, B. A model of physiological adaption in unicellular algae. *J. Theor. Biol.* **78,** 519–552 (1979).

29. Raven, J. A. & Geider, R. J. Temperature and algal growth. *New Phytol.* **110,** 441–461 (1988).

30. Raven, J. A. The Quantitative Role of ' Dark ' Respiratory Processes in Heterotrophic and Photolithotrophic Plant Growth. *Ann. Bot.* **40**, 587–602 (1976).

31. Geider, R. J. & Osborne, B. A. Respiration and microalgal growth□: a review of the quantitative relationship. *New Phytol.* **112,** 327–341 (1989).

32. Mathur, S., Agrawal, D. & Jajoo, A. Photosynthesis: Response to high temperature stress. *J. Photochem. Photobiol. B Biol.* **137,** 116–126 (2014).

33. Marañón, E., Lorenzo, M. P., Cermeño, P. & Mouriño-Carballido, B. Nutrient limitation suppresses the temperature dependence of phytoplankton metabolic rates. *ISME J.* (2018). doi:10.1038/s41396-018-0105-1

34. Thomas, M. K. *et al.* Temperature–nutrient interactions exacerbate sensitivity to warming in phytoplankton. *Glob. Chang. Biol.* **23,** 3269–3280 (2017).

35. Graham, J. M., Auer, M. T., Canale, R. P. & Hoffmann, J. P. Ecological Studies and Mathematical Modeling of Cladophora in Lake Huron: 4. Photosynthesis and Respiration as Functions of Light and Temperature. *J. Great Lakes Res.* **8,** 100–111 (1982).

36. Davison, I. R. Environmenal effects on algal photosynthesis: Temperature. *J. Phycol.* **27,** 2–8 (1991).

37. Listmann, L., LeRoch, M., Schlüter, L., Thomas, M. K. & Reusch, T. B. H. Swift thermal reaction norm evolution in a key marine phytoplankton species. *Evol. Appl.* **9,** 1156–1164 (2016).

38. Schaum, C.-E., Buckling, A., Smirnoff, N., Studholme, D. J. & Yvon-Durocher, G. Environmental fluctuations accelerate molecular evolution of thermal tolerance in a marine diatom. *Nat. Commun.* 1–14 (2018). doi:10.1038/s41467-018-03906-5

Acknowledgements

This study was supported by a grant from the Leverhulme Trust (RPG-2013-335) awarded to G.Y.-D., A.B. and N.S.

Author contributions

S.B. and G.Y.-D conceived the study. S.B., G.Y.-D, A.B. and N.S. designed the experimental work. S.B., J.J. and C.-E.S. conducted the experimental work. S.B. and G.Y.-D analysed the data. S.B. and G.Y.-D wrote the manuscript and all authors contributed to revisions.

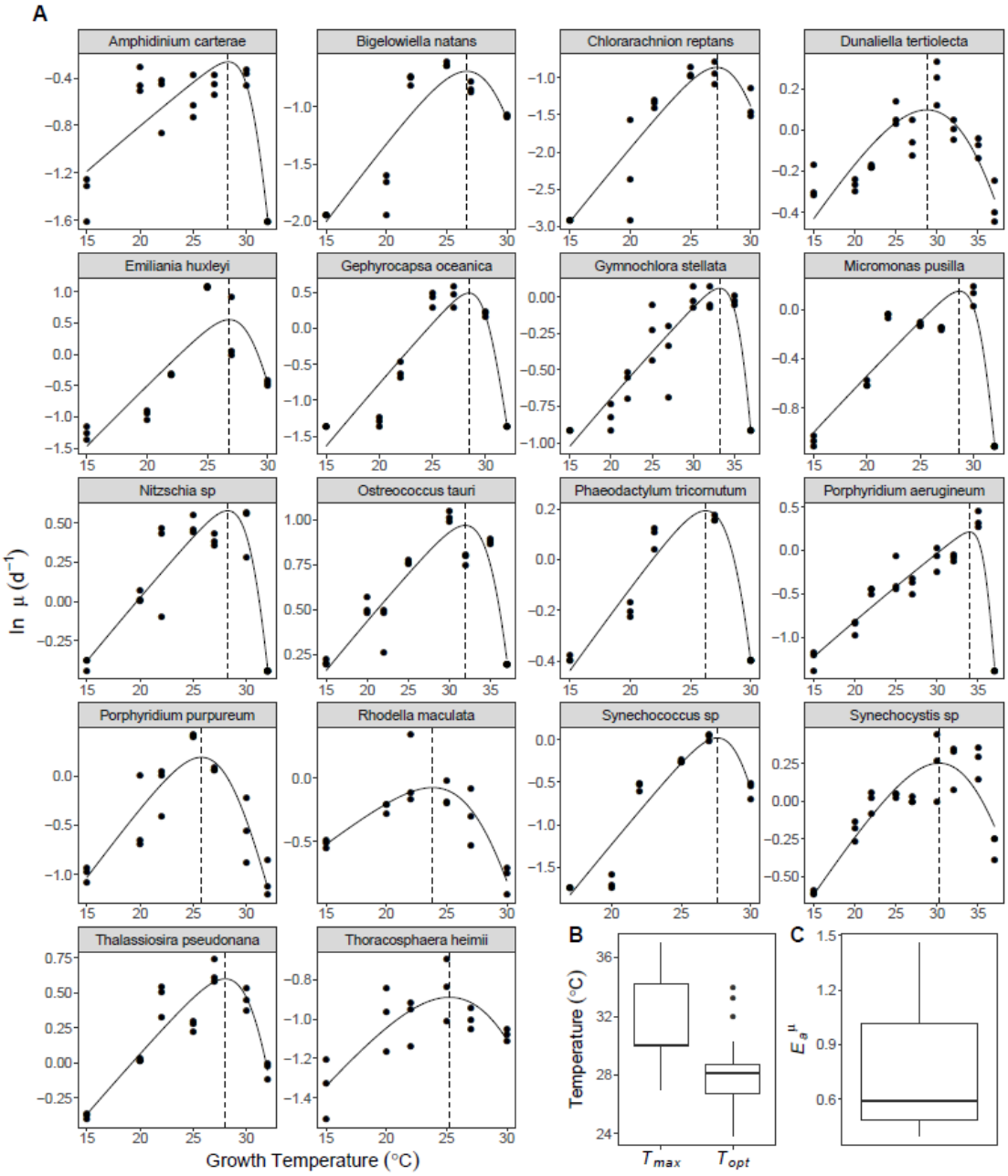

Figure 1 | Thermal tolerance curves for 18 species of marine phytoplankton. (A) Thermal reaction norms for all 18 species used in this study. The data points presented are the natural logarithm of per capita growth rate, μ, for each replicate (n= minimum of 3 technical replicates per assay temperature for each species). The fitted lines are from the predicted random effect of species derived from non-linear mixed effects modelling with a Sharpe-Schoolfield model. The vertical dashed lines correspond with the optimal temperatures of growth. **(B)** Boxplot distributions of optimal growth temperatures (T_{opt}) and maximum temperatures of growth (T_{max}) across all 18 species. **(C)** Boxplot distribution of growth activation energy, or temperature dependence ($E_a{}^{\mu}$), across all 18 species (Table 2, SI). The bold horizontal line corresponds to the median value, the top and bottom of the box correspond to the 75th and 25th percentiles and the whiskers extend to the largest and smallest values no greater or less than 1.5 $\times$ the interquartile range, beyond which the points are plotted as outliers.

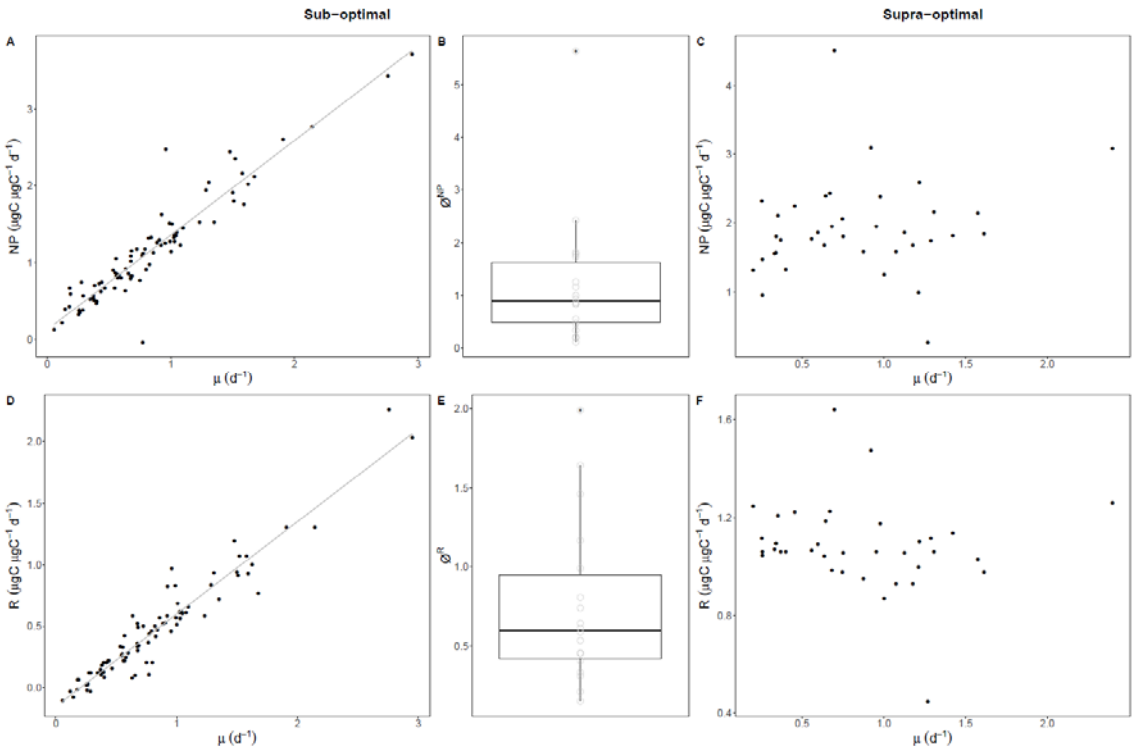

Figure 2 | Coupling between metabolism and growth. (A) A scatter plot of the net photosynthesis rates at each sub-optimal growth temperature against the respective per capita growth rate for all 18 species. The fitted line represents the fixed effect slope coefficient, $\emptyset^{NP}$, from linear mixed effects modelling. **(B)** Boxplot with overlaying data points (grey circles) for the species-specific $\emptyset^{NP}$ values derived from the random effects of the linear mixed effects model (Table 7, SI). **(C)** Net photosynthesis rates were decoupled from growth rates at supra-optimal growth temperatures. **(D)** Dark respiration rates were coupled to rates of growth for all 18 species at sub-optimal growth temperatures. **(E)** Boxplot of the species-specific $\emptyset^{R}$ values derived from the random effect output of the linear mixed effects model (Table 7, SI). **(F)** Dark respiration rates were decoupled from growth rates at supra-optimal growth temperatures. For A, C, D and F metabolic rates have been standardised by dividing rates by the species specific intercept for visualisation of the data only. In all boxplots the bold horizontal line corresponds to the median value, the top and bottom of the box correspond to the 75th and 25th percentiles and the whiskers extend to the largest and smallest values no greater or less than 1.5 $\times$ the interquartile range, beyond which the points are plotted as outliers.

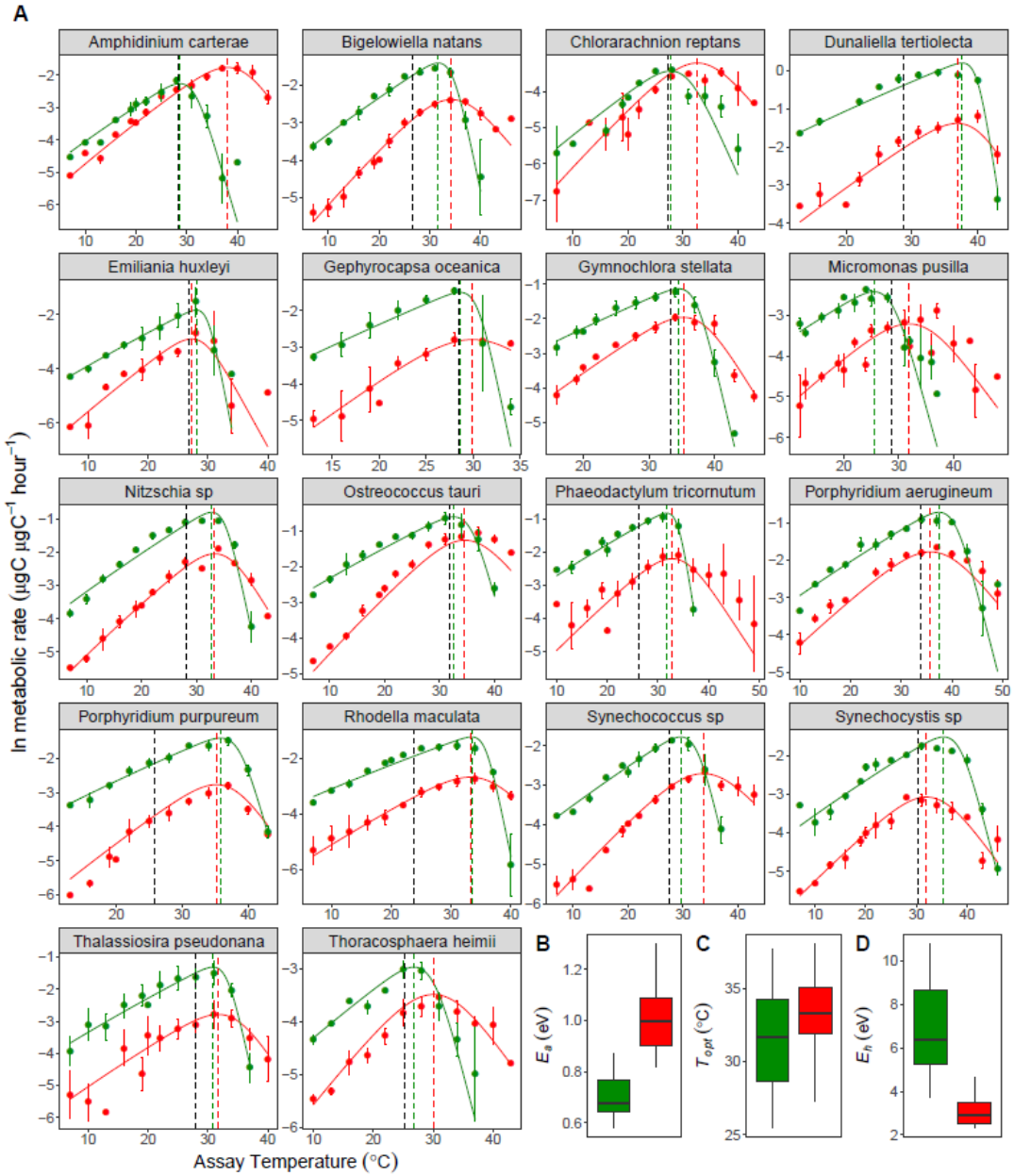

Figure 3| Thermal performance curves for respiration and gross photosynthesis in 18 species of marine phytoplankton. (A) Metabolic thermal performance curves for all 18 species used in this study. Green colouring denotes gross photosynthesis, red colouring denotes respiration. The data points presented are the natural logarithm of mean metabolic, with error bars denoting ± s.e.m (n = minimum of 3 biological replicates per response for each species). The fitted lines for each species are from the random effects of a non-linear mixed effects model fitted to the rate data using the Sharpe-Schoolfield equation (see Methods). The vertical dashed lines correspond with the optimal temperatures for each metabolic flux, with the black dashed line added to show optimal growth temperature. **(B, C and D)** Boxplots showing the distribution of the estimated values for activation energy (E_a), optimal temperature (T_{opt}) and deactivation energy (E_h) for photosynthesis and respiration across the 18 species (Tables 4 and 5, SI). The bold horizontal line corresponds to the median value, the top and bottom of the box correspond to the 75th and 25th percentiles and the whiskers extend to the largest and smallest values no greater or less than 1.5 × the interquartile range, beyond which the points are plotted as outliers.

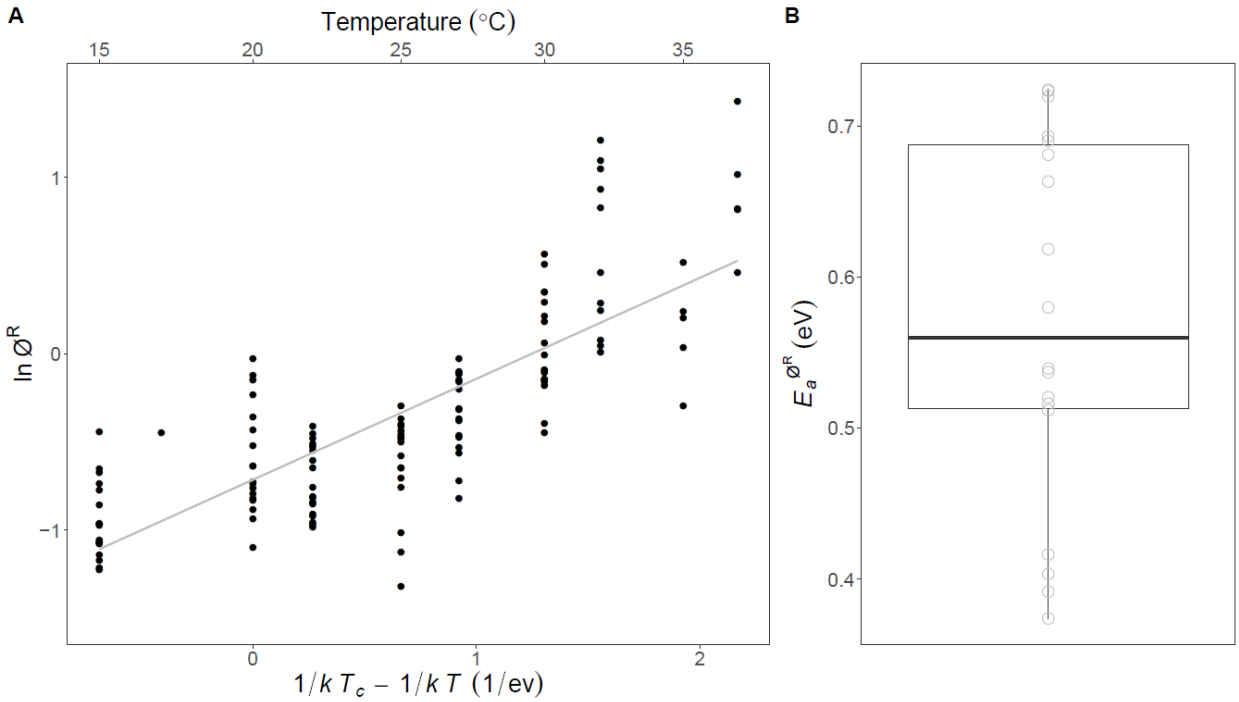

Figure 4 | The temperature dependence of the respiratory costs of biomass synthesis. (A) A scatterplot showing the relationship between the natural logarithm of the respiratory cost of biosynthesis, $\emptyset^R$, and standardised Boltzmann temperature for the pooled dataset of 18 species, where T_c = 20°C and k is the Boltzmann constant (8.62×10^{-5} eV). The fitted line represents the fixed effect of a linear mixed effects model fitted to the data using the Boltzmann-Arrhenius equation (see Methods). Values of $\emptyset^R$ have been standardised by dividing by the species-specific intercept derived from the random effects of the mixed effects model. This standardisation was for visualisation of the data only. The plot demonstrates that the overall respiratory cost of biomass synthesis increases exponentially with rising temperature across the full range of growth temperatures ($\chi^2 = 30.0$, $p < 0.005$). **(B)** Boxplot of the species-specific activation energies, ${E_a}^{\emptyset^R}$, characterising the temperature dependence of $\emptyset^R$. This value was positive for all 18 species indicating that the cost of synthesis increased with temperature, with an average value across species of ${E_a}^{\emptyset^R}$ = 0.57eV (Table 8, SI). The bold horizontal line corresponds to the median value, the top and bottom of the box correspond to the 75th and 25th percentiles and the whiskers extend to the largest and smallest values no greater or less than 1.5 × the interquartile range, beyond which the points are plotted as outliers.

METHODS

Culturing of marine phytoplankton strains

18 marine phytoplankton strains were obtained from CCAP (The Culture Collection of Algae and Protozoa) and RCC (Roscoff Culture Collection) between autumn 2015 and spring 2016. Strains of eukaryotic phytoplankton were selected from phylogenetic groups of both the red and green superfamilies[1,2], in addition to two strains of cyanobacteria. We tried to work with organisms that had been well studied in the literature, were known to be globally abundant and play crucial roles for marine ecology and global carbon cycling. The strains were originally isolated from a range of latitudes and some have been in culture for up to 65 years (Table 1, SI).

Stocks of each of the strains were cultured on their previous culture collection medium (Table 1, SI) using artificial sea water. The following media were used: Guillard's F/2 and F/2 + Si, Keller's K, K + Si and K/2, and PCR-S11 Red Sea medium (with Red Sea salts).

All stock cultures were incubated in Infors HT incubators at 20°C, under a 12:12 hour light-dark cycle with a PAR intensity of 45-50 µmol $m^2 s^{-1}$ and shaken at 65RPM. Where possible we tried to obtain strains from the culture collections that matched, or were close to, these conditions. The red alga *Porphyridium purpureum* was an exception, which we cultured at 20-25 µmol $m^2 s^{-1}$. Cultures were kept under exponential, nutrient replete, growth conditions for ~ 2 months before any physiological data was collected.

Measuring the thermal tolerance curve

For each species, a minimum of 3 technical replicates were inoculated with the same starting density into fresh growth medium across a range of temperatures (15°C - 37°C). Cell counts were made daily using flow cytometry (Accuri C6 flow cytometer, BD Scientific), and

population density was tracked until cultures reached carrying capacity. Per capita growth rates (μ) were quantified from a modified Baranyi growth model without the lag phase[3], using non-linear least squares regression via the 'nlsMicrobio' package in R statistical software (v3.3.1). Models were fitted using the 'nlsLoop' function in the R github package 'nlsLoop'. This draws on the 'nlsLM' function in the 'minpack.lm' R package, which uses a modified Levenberg-Marquardt optimisation algorithm. Model parameters were determined by running 2000 random combinations of estimated starting parameters, which were then selected using the Akaike Information Criterion (AIC) to determine the set of parameters that best characterised the data. Growth rates derived for each technical replicate at each growth temperature were then used to determine the thermal tolerance curves (Fig.1A).

Estimates of Cell Carbon and Nitrogen

For each species, an exponentially growing culture from the 20°C stock was divided into 3 technical replicates and centrifuged at 3500RPM, at 4°C for 30 minutes. The resultant pellets were rinsed with deionised water and re-spun 3 times to remove any artificial sea water residue. For the calcifying organisms (*Emiliania huxleyi, Gephyrocapsa oceanica, Thoracosphaera heimii* i.e. those with a calcium carbonate coccoliths) it was necessary to dissolve the extra-cellular inorganic carbon. This was achieved by treating these pellets with 0.5 mL of 3M HCl for 1 hour before being rinsed with deionised water and re-pelleted [4,5].

All pellets were freeze-dried using a CoolSafe (95-15 PRO, ScanVac) over 24 hours and then weighed to obtain dry weight. Samples were placed in tin cups and sent to Elemtex (Elemtex Ltd, Cornwall, UK, PL17 8QS) for elemental analysis of %C and %N using a SerCon Isotope Ratio Mass Spectrometer (CF-IRMS) system (continuous flow mode). For each technical replicate we then calculated the C:N ratio as well as $\mu g\ C\ cell^{-1}$ (Table 3, SI).

Measuring the metabolic thermal response curves

Measurements of photosynthesis and dark respiration were collected across a range of assay temperatures (7°C to 50°C) for a minimum of 3 biological replicates per species. We used a clark-type oxygen electrode as part of a Chlorolab 2 system (Hansatech Ltd, King's Lynn, UK) to measure net rates of oxygen evolution in the light (net primary production, NP) and oxygen consumption in the dark (dark respiration); both in units of µmol O_2 mL^{-1} s^{-1}. All biological replicates were sampled from the stock cultures, which had all been growing at 20°C and were taken at the mid-logarithmic growth phase to ensure that the samples were not substrate limited. To improve the signal to noise ratio when measuring rates, all biological replicate samples were concentrated by centrifugation at 1500rpm, 20°C, for 15 minutes and re-suspended into an adequate volume of fresh growth medium. Prior to running a sample at each assay temperature, all samples were given ~ 15 minutes to pre-acclimate to the assay temperature in the dark before any data was collected. This also gave the electrode system sufficient time to stabilise before metabolic rates were measured. This was necessary for two reasons, i) as the sample adjusts to the assay temperature this will naturally cause changes in the dissolved oxygen concentration, ii) the electrode system results in oxygen signal drift, and this too is temperature dependent. We measured rates of oxygen depletion from 23 sterilised artificial seawater samples across a range of temperatures 4°C - 44°C and found that the impact of drift was minimised after ~15 minutes of stabilisation time. Nevertheless, signal drift was linearly temperature dependent after this time. To account for drift in our dataset we corrected all our raw data using the following empirically derived relationship:

$$drift = (-0.389 \times T) - 5.50 \qquad (1)$$

Where T is assay temperature (°C), and *drift* is the non-biological depletion in oxygen concentration measured in units µmolO_2 mL^{-1} s^{-1} after approximately 15 minutes of stabilisation. The raw O_2 flux data was then corrected by subtracting the estimated drift.

Rates of net photosynthesis, measured as O_2 evolution, were collected across a range of light intensities from 0 to 1800 µmol m^2 s^{-1} with increments of 50 µmol m^2 s^{-1} between 0 to 200 µmol m^2 $s^{-1,}$ 100 µmol m^2 s^{-1} between 200 and 1000 µmol m^2 s^{-1}, followed by 1200 µmol m^2 s^{-1}, 1500 µmol m^2 s^{-1} and finally 1800 µmol m^2 s^{-1}. This enabled us to model a photosynthesis-irradiance (PI) curve for each assay temperature, and therefore obtain an estimate of light saturated net photosynthesis, NP_{max}, see Eq. 2. Respiration (*R*) was measured as oxygen consumption in the dark, over a 3-minute period directly following the light response outlined above. The photosynthesis-irradiance curve was then quantified by fitting Eiler's photoinhibiton model to the data using non-linear least squares regression (as described above)[6,7]:

$$NP(I) = \frac{NP_{max} I}{\frac{NP_{max}}{\alpha I_{opt}^{2}} I^2 + \left(1 - 2\frac{NP_{max}}{\alpha I_{opt}}\right) I + \frac{NP_{max}}{\alpha}} \qquad (2)$$

Where $NP(I)$ is the rate of net primary production at light intensity, I, NP_{max} is the maximum rate of NP at the optimal light intensity, I_{opt}, and α is the rate in which NP increases up to NP_{max}.

Light saturated gross primary production (*P*) was then calculated for each assay temperature as:

$$P = NP_{max} + R \qquad (3)$$

Metabolic rates were then converted from units µmol O_2 mL^{-1} s^{-1} to µg C µg C^{-1} $hour^{-1}$. We achieved this using the following equation:

$$b(\mu g\ C\ \mu g\ C^{-1}\ h^{-1}) = \frac{b(\mu mol\ O_2\ cell^{-1}\ h^{-1}) \times 32 \times M \times (\frac{12}{44})}{\mu g C\ cell^{-1}} \qquad (4)$$

Where b is the metabolic rate (either P or R), 32 is the molecular weight of O_2, M is a species specific assimilation quotient for CO_2:O_2[8] which is used to describe consumption or fixation of C in the cell per unit of O_2 , and 12/44 is the ratio of molecular weight of C to CO_2, thus $32 \times M \times \frac{12}{44}$ converts from $\mu mol\ O_2$ to μgC. Samples from each strain were analysed to determine species-specific $\mu g\ C\ cell^{-1}$ values and the number of cells mL^{-1} was measured for each biological replicate using flow cytometry. The calculation of M is based on the assumption that NO_3^- is the main nitrogen source in the growth medium and that there is a balanced growth equation, where:

$$nCO_2 + (n+1)H_2O + HNO_3 \rightarrow (CH_2O)_n\ NH_3 + (n+2)O_2 \qquad (5)$$

If the C:N ratio (n) of the phytoplankton is calculated in moles then the ratio of CO_2:O_2, or M, will be equal to $n/n+2$ [8]. Our calculated values of M ranged from ~0.71 to ~0.89 (Table 3, SI).

<u>Quantifying the thermal response curves</u>

The thermal response curves for rates of growth, photosynthesis and respiration were quantified using a modified version of the Sharpe-Schoolfield equation[9,10]:

$$\ln\big(b(T)\big) = E_a\left(\frac{1}{kT_c} - \frac{1}{kT}\right) + \ln\big(b(T_c)\big) - \ln\left(1 + e^{E_h\left(\frac{1}{kT_h} - \frac{1}{kT}\right)}\right) \qquad (6)$$

where b is either the rate of growth (d^{-1}), photosynthesis or respiration ($\mu g\ C\ \mu g\ C^{-1}\ h^{-1}$), k is Boltzmann's constant (8.62×10^{-5} eV K^{-1}), E_a is the activation energy (eV), indicative of the steepness of the slope leading up to the thermal optima, T is temperature in Kelvin (K), E_h is the deactivation energy which characterizes temperature-induced decrease in rates above T_h where half the enzymes have become non-functional and $b(T_c)$ is rate normalized to an arbitrary reference temperature, here T_c = 20ºC (+ 273.15), where no low or high temperature inactivation is experienced. Eq. 6 can be used to derive an optimum temperature where the

maximum rate is predicted:

$$T_{opt} = \frac{E_h T_h}{E_h + kT_h \ln\left(\frac{E_h}{E_a} - 1\right)} \quad (7)$$

The parameters $b(T_c)$, E_a, E_h, T_h, and T_{opt}, can be considered as traits that characterise the unimodal response of biological rates to temperature change. We expect these traits to differ across the diverse taxa analysed in this study, owing to their diverse evolutionary histories and ancestral temperature regimes (given that they have been isolated from different latitudes/oceans). To test this assumption, we fitted the data for growth, photosynthesis and respiration across all species to Eq. 6 using non-linear mixed effects modelling with the 'nlme' package in R. We used separate analyses to assess the thermal responses of growth, photosynthesis and respiration. All models included each of the parameters in Eq. 6 as fixed effects, which quantify the average value of the parameter across all species and replicates. For the analysis of the thermal response of growth rate, we included 'species' as a random effect on each parameter, which quantifies species-specific deviations from the average across all species (i.e. the fixed effect) that are assumed to be normally distributed with a mean of zero. For the analyses of photosynthesis and respiration, we included 'replicate' nested within 'species' to account for the fact that we measured a minimum 3 replicate thermal response curves for each species. Here the random effect quantifies species-specific deviations from the fixed effects as well as those attributable to variance among the replicates of each species.

Linking metabolism and growth

To assess the coupling between metabolic rate and the rate of population growth necessitates scaling up the metabolic rates measured in the O_2 electrode system on the order of minutes to the rates of per capita growth rate measured over several days across a 12:12h light/dark

cycle. Per capita growth has units of d^{-1}. To derive metabolic rates in comparable units we scaled the rates of *R* and *NP* over the 12:12h light/dark cycle by multiplying each by 12h – i.e. the number of hours under irradiance and dark conditions over the 24h cycle. This yielded rates of the *R* and *NP* in units of µg C µg C^{-1} d^{-1}, which can be simplified to units of d^{-1} by cancelling the units of C. Out of the 18 species investigated, 4 species (*Chlorarachnion reptans, Gephyrocapsa oceanica, Ostreococcus tauri* and *Porphyridium aerugineum*) returned values of metabolism that when scaled up to diurnal rates were an order of magnitude higher or lower than the growth rates. This divergence could be attributed to erroneously high or low estimates of cellular carbon, which were also different to previously published estimates for organisms of a comparable cell size, by an order of magnitude. For these four organisms we replaced our carbon $\mu gC\ cell^{-1}$ measurements with an estimated value derived for cells of a similar volume using a well established scaling relationship between carbon content and cell biovolume[11]. Confocal microscope images in conjunction with ImageJ software were used to estimate bio-volume from geometric models for marine phytoplankton that most resembled for morphology of each species[12,13].

There are several sources of error that might lead to inaccuracies in the upscaling of the physiological rates to rates of growth measured in culture. First, we have to assume that rates of photosynthesis and respiration measured in a small aliquot in a separate chamber to the culture are representative of the light, thermal and physical conditions in the culture vessel. Small differences in conditions between the respirometry chamber and the culture vessel could lead to inaccuracies in the upscaling of physiological rates. Second, the time scale of the measurements of photosynthesis and respiration are on the order of minutes, whilst the rates of population growth represent an average over several days. There are currently no technical solutions to resolve these methodological challenges experimentally. Indeed similar constraints have been recognised in the algal physiology literature for many decades[8,14,15].

Our measurements of photosynthesis and respiration therefore represent the best possible estimates of the physiological processes under the culture conditions, but they must be interpreted as estimates that have a degree of error that reflect the limitations of the method.

To quantify the coupling between growth and metabolism, we used a simple model of growth energetics[14], which assumes that at sub-optimal temperatures, the rate of growth is proportional to the rate of metabolism

$$b = \emptyset\mu + b_0 \qquad (8)$$

where b is the rate of metabolism (either net photosynthesis or respiration), $\emptyset$ is the metabolic cost of growth, μ is growth rate and b is the maintenance metabolism[14]. There is currently no clear consensus in the literature about the precise nature of the coupling between photosynthesis, respiration and growth, with some studies arguing for the role of dark respiration in biosynthesis, while others emphasise the importance of ATP and reductant for growth provided by photosynthesis[14,16]. Here we analyse the coupling between all three variables to investigate the physiological constraints on the thermal tolerance of growth. We fitted Eq. 8 in two separate analyses to the measurements of net photosynthesis/respiration (in place of the b parameter) and μ below the optimal temperature for growth for each species using linear mixed effects models, fitted via the 'lme' function in the 'nlme' R package. We treated $\emptyset$ and b_0 as fixed effects, which model their average value across the 18 species. We also included random effect of species on $\emptyset$ and b_0 (i.e. the slope and intercept respectively), which allowed us to capture the species-specific coupling between metabolism and growth as well as the 'average' relationship across all species.

We also investigated the direct coupling between dark respiration and gross photosynthesis. Respiration is ultimately limited by the supply carbohydrates fixed by

photosynthesis and is therefore expected to be linearly dependent on rates of gross photosynthesis

$$R = \varepsilon P + R_0 \qquad (9)$$

where R is the rate of dark respiration, P is the rate of gross photosynthesis, ε is the fraction of carbon fixed by P accounted for by R and R_0 is the rate of dark respiration when gross photosynthesis is zero. We fitted Eq.9 to the measurements of R and P both below and above ${T_{opt}}^{\mu}$ for each species using a linear mixed effects modelling, thus allowing us to compare the coupling at sub-optimal and supra optimal growth temperatures. We treated ε and R_0 as fixed effects, which model their average value across the 18 species. We also included random effects on ε and R_0 (i.e. the slope and intercept respectively), which allowed us to capture the species-specific coupling between R and P as well as the 'average' relationship across all species (see Fig. S4).

For each of the 18 species of marine phytoplankton, we measured R and μ across a temperature gradient (Fig. 1 and 3). We can therefore rearrange Eq.8 to assess how $\emptyset^R$ (the respiratory cost of biosynthesis) varies with temperature

$$\emptyset^R(T) = R(T) - R_0 / \mu(T) \qquad (10)$$

where $R(T)$ is the predicted R value derived from the species level thermal response curve for respiration at growth temperature, T, μ is the mean growth rate measured at T , and R_0 is the maintenance respiration rate when μ= 0.

We characterised the temperature-dependence of $\emptyset^R$ using the Arrhenius equation,

$$\ln\emptyset^R(T) = {E_a}^{\emptyset^R}\left(\frac{1}{kT_c} - \frac{1}{kT}\right) + \ln\emptyset^R(T_c) \qquad (11)$$

where $\ln\emptyset^R(T)$ is the natural logarithm of the cost synthesis at temperature T (in Kelvin), ${E_a}^{\emptyset^R}$ is the apparent activation energy characterising the temperature dependence of $\emptyset^R$. We

centred the temperature data using an arbitrary reference temperature T_c = 283 K = 20ºC, so that $\ln\emptyset^R(T_c)$ is the cost of synthesis at T_c. We fitted Eq. 11 to the measurements of $\emptyset^R$ using a linear mixed effects model. We treated ${E_a}^{\emptyset^R}$ and $\ln\emptyset^R(T_c)$ as fixed effects, which model their average value across the 18 species. We also included random effects on ${E_a}^{\emptyset^R}$ and $\ln\emptyset^R(T_c)$ (i.e. the slope and intercept respectively), which allowed us to capture the species-specific temperature dependence of $\emptyset^R$ as well as the 'average' relationship across all species.

References

1. Keeling, P. J. Diversity and evolutionary history of plastids and their hosts. *Am. J. Bot.* **91,** 1481–1493 (2004).

2. Falkowski, P. G. *et al.* The Evolution of Modern Eukaryotic. *Science,* **305,** 354–360 (2004).

3. Baranyi, J. & Roberts, T. A. A dynamic approach to predicting bacterial growth in food. *Int. J. Food Microbiol.* **23,** 277–294 (1994).

4. Ho, T. *et al*. the Elemental Composition of Some Marine Phytoplankton. *J. Phycol*. **39,** 1145–1159 (2003).

5. Biermann, A. & Engel, A. Effect of CO_2 on the properties and sinking velocity of aggregates of the coccolithophore Emiliania huxleyi, *Biogeosciences.* **7,** 1017–1029 (2010).

6. Eilers, P. H. C. & Peeters, J. C. H. A model for the relationship between light intensity and the rate of photosynthesis in phytoplankton. *Ecol. Modell.* **42,** 199–215 (1988).

7. Edwards, K. F., Thomas, M. K., Klausmeier, C. a. & Litchman, E. Phytoplankton growth and the interaction of light and temperature: A synthesis at the species and community level. *Limnol. Oceanogr*. **61,** 1232–1244 (2016).

8. Falkowski, P. G., Dubinsky, Z. & Wyman, K. Growth-irradiance relationships in phytoplankton . *Limnol. Oceanogr*. **30,** 311–321 (1985).

9. Sharpe, P. J. H. & DeMichele, D.W. Reaction Kinetics of Poikilotherm Development. *J. Theor. Biol.* **64,** 649–670 (1977).

10. Schoolfield, R. M., Sharpe, P. J. H. & Magnuson, C. E. Non-linear regression of biological temperature-dependent rate models based on absolute reaction-rate theory. *J. Theor. Biol.* **88,** 719–731 (1981).

11. Montagnes, D. J. S., Berges, J. a., Harrison, P. J. & Taylor, F. J. R. Estimating carbon, nitrogen, protein, and chlorophyll a from volume in marine phytoplankton. *Limnol. Oceanogr.* **39,** 1044–1060 (1994)

12. Hillebrand, H., Dürselen, C.-D., Kirschtel, D., Pollingher, U. & Zohary, T. Biovolume Calculation for Pelagic and Benthic Microalgae. *J. Phycol.* **35,** 403–424 (1999).

13. Sun, J. & Liu, D. Geometric models for calculating cell biovolume and surface area for phytoplankton. *J. Plankton Res.* **25,** 1331–1346 (2003).

14. Geider, R. J. & Osborne, B. A. Respiration and microalgal growth□: a review of the quantitative relationship. *New Phytol.* **112,** 327–341 (1989).

15. Marañón, E., Lorenzo, M. P., Cermeño, P. & Mouriño-Carballido, B. Nutrient limitation suppresses the temperature dependence of phytoplankton metabolic rates. *ISME J.* (2018). doi:10.1038/s41396-018-0105-1

16. Raven, J. A. The Quantitative Role of 'Dark' Respiratory Processes in Heterotrophic and Photolithotrophic Plant Growth. *Ann. Bot.* **40**, 587–602 (1976).